Numerical simulation of unsteady cavity flow using Lattice Boltzmann Method*

Denis Ricot†, Virginie Maillard‡ and Christophe Bailly§

†, ‡ Direction de la Recherche, Renault S.A.
TCR RUC 4 05, 1 avenue du golf
78288 Guyancourt cedex, France.

§ Laboratoire de Mécanique des Fluides et d'Acoustique
Ecole Centrale de Lyon & UMR CNRS 5509
BP 163, 69131 Ecully cedex, France.

Abstract

A lattice Bolzmann code based on the two-dimensional nine-velocity model has been developed for computational aeroacoustic studies. The connection between the continuous and lattice Boltzmann equations is completely described for this model. A discrete-velocity Boltzmann equation is first constructed and is integrated along a characteristic. The fully explicit equations of the LBM are recovered by introducing equivalent distribution functions. Using the discrete velocity Boltzmann equation, a free field boundary is proposed to minimize the reflection of vortical and acoustic perturbations on the limit of the calculation domain. The numerical stability problem for under-resolved sheared flow is overcome by adding a selective viscosity filter that damps the spurious high frequency numerical oscillations. The first validation cases are the pulse propagation in a uniform flow and a cavity excited by a laminar grazing flow. The results show that the LBM could be used for aeroacoustic computations of low subsonic flows.

1. Introduction

The lattice Boltzmann method (LBM) is an innovative numerical method based on kinetic theory to simulate various hydrodynamic systems. The scheme is particularly successful in fluid applications[10] involving interfacial dynamics, multiphase, multicomponent flows and particle suspension which are usually difficult problems for traditional numerical schemes. But in its simplest form, the lattice Boltzmann method simulates the time-dependent motion of a perfect gas at low Mach number that is governed by the compressible Navier-Stokes equations. Then, LBM is a reasonable candidate for simulations of turbulence, flow-induced noise and sound propagation. For example, the response of a two-dimensional Helmholtz cavity under grazing flow has been investigated[32] with the commercial code PowerFLOW based on the LBM. The acoustic coupling between the vortex shedding and the cavity resonance has been predicted by the solver. This preliminary result encouraged the authors to study in more details this numerical method in the framework of computational aeroacoustics.

The development of the lattice Boltzmann equation (LBE) was independent of the continuous Boltzmann equation. It was introduced[9,29] to solve some of the difficulties of the Lattice Gas Automata (LGA).[16] A parameter matching procedure (see appendix of reference [23]) based on the Chapman-Enskog analysis of the LGA allowed to construct a set of relaxation equations so that the correct hydrodynamic equations are derived. But recently, the connection between the LBE models and the continuous Boltzmann equation has been explicitly shown.[1,21] This new approach is presented in the second part of this paper. The boundary conditions for aeroacoustic simulations are investigated in the third part. The stability problem of LBM for low viscosity is discussed in part 4. Then, the aeroacoustic test case of a pulse in a uniform flow is studied in part 5. In part 6, the self-sustained oscillation of a laminar flow over a rectangular cavity is calculated.

2. Theory of the Lattice Boltzmann Method

2.1 The continuous Boltzmann equation

In kinetic theory,[24] a monoatomic gas is represented as a cloud of like point particles and is fully described by its continuous distribution function $f_m(\mathbf{x}, \mathbf{c}, t)$, which represents the number of particles whose positions and velocities are $\mathbf{x}$ and $\mathbf{c}$ at time t. Then we can define a the density distribution function $f(\mathbf{x}, \mathbf{c}, t) = m f_m(\mathbf{x}, \mathbf{c}, t)$, with m the molecular mass of the gas. It is a mesoscopic description of the fluid, intermediate between the micro-

†PhD student

‡Research Engineer, Renault S.A.

§Assistant Professor, Member AIAA

scopic and macroscopic ones. For a dilute (or rarefied) gas where only binary collisions between particles occur, the evolution of the distribution function is governed by the Boltzmann equation[6] :

$$\frac{\partial f}{\partial t} + c_i \frac{\partial f}{\partial x_i} = \Omega(f) \tag{1}$$

where $\Omega(f)$ is a bilinear collision operator which determines physics of the flow. The fluid density ρ, velocity $\mathbf{u}$ and internal energy e are defined via moments of the distribution function :

$$\rho = \int f d\mathbf{c} \tag{2}$$

$$\rho \mathbf{u} = \int \mathbf{c} f d\mathbf{c} \tag{3}$$

$$\rho e + \frac{1}{2}\rho |\mathbf{u}|^2 = \frac{1}{2}\int |\mathbf{c}|^2 f d\mathbf{c} \tag{4}$$

In case of elastic collisions, the mass, momentum and kinetic energy are conserved. For the collision operator $\Omega(f)$ to be mass, momentum and energy conservative, it is required that

$$\int \Psi_p \Omega(f)\, d\mathbf{c} = 0 \tag{5}$$

for $\Psi_0 = 1, \Psi_1 = c_1, \Psi_2 = c_2, \Psi_3 = c_3, \Psi_4 = |\mathbf{c}|^2$, which are frequently called the elementary collision invariants. Hence, it is possible to derive all the continuous equations by multiplying the Boltzmann equation (1) by Ψ_p, $p = 0, ..., 4$ and integrating over all velocities. Using relations (2), (3) and (4), we obtain successively :

$$\begin{gathered} \frac{\partial \rho}{\partial t} + \frac{\partial \rho u_i}{\partial x_i} = 0 \\ \frac{\partial \rho u_j}{\partial t} + \frac{\partial (\rho u_i u_j + P_{ij})}{\partial x_i} = 0 \\ \frac{\partial \left[\rho \left(\frac{1}{2}u^2 + e\right)\right]}{\partial t} + \frac{\partial \left[\rho u_i \left(\frac{1}{2}u^2 + e\right) + P_{ij} u_j + q_i\right]}{\partial x_i} = 0 \end{gathered} \tag{6}$$

where P_{ij} is the total stress tensor and $\mathbf{q}$ is the heat flux which expressions depend on $\mathbf{c}$ and f :

$$P_{ij} = \int (c_i - u_i)(c_j - u_j) f d\mathbf{c} \tag{7}$$

$$q_i = \frac{1}{2}\int (c_i - u_i) |\mathbf{c} - \mathbf{u}|^2 f d\mathbf{c} \tag{8}$$

It is worth noting that the derivation of these equations does not depend on the exact form of the collision operator. Of course, the above conservation equations are *not* the hydrodynamic equations : the stress tensor and heat flux cannot be a priori computed only in term of ρ, $\mathbf{u}$ and e. The closure problem consists in finding such relations and it was tackled via the expansion methods of Chapman-Enskog[7] and Hilbert. Rigorous mathematical derivation of compressible Navier-Stokes equations with formal expressions of the transport coefficients (shear and bulk viscosities, heat conductivity) can be found in literature.[4,15,19] In this paper, the general outlines of the Chapman-Enskog (or Hilbert) expansion will be given within the framework of discrete-velocity Boltzmann equation with the nine-speed model and a simplified collision operator.

Boltzmann's equation can be use to derive the fundamental conservation laws but it also contains a natural notion of entropy and entropy production. This can be seen by considering the function $H(t) = \int f \ln f d\mathbf{c}$. The entropy of the system can be written as $S(t) = -k_B H(t) + \alpha$, where k_B is the Boltzmann's constant and α is also a constant. Differentiating H with respect to time and using Boltzmann's equation to replace the time derivative of f in the integral, it can be shown[7] that $\partial H/\partial t \leq 0$. This means that H can never increase, and consequently that the entropy can never decrease, and is known as Boltzmann's H-theorem. It can be also shown that H is bounded below. Then H decreases until f reaches an equilibrium state f^{eq} defined by $\partial H/\partial t = 0$. Solutions of this equation are the global (constant in both time and space) and local Maxwellian equilibrium functions. The local Maxwellian is :

$$f^{eq} = \rho \left(\frac{m}{2\pi k_B T}\right)^{D/2} \exp\left[\frac{-m|\mathbf{c} - \mathbf{u}|^2}{2k_B T}\right] \tag{9}$$

with T the fluid temperature and D the spatial dimension. We introduce the normalized temperature $\theta = rT$, with r the gas constant given by $r = k_B/m$.

The complicated analytical form of the particle collision term $\Omega(f)$ leads to tedious calculations for the closure problem. In fact, a large amount of the details of the two-body interaction is unlikely to influence significantly the values of macroscopic quantities. It is therefore assumed[6] that $\Omega(f)$ can be replaced by a simplified collision operator. The H-theorem shows that the collision operator drives the distribution function f toward the local Maxwell-Boltzmann equilibrium distribution f^{eq}. The most straightforward choice of collision operator is the linearized collision operator with a single relaxation time λ or the Bhatnagar-Gross-Krook (BGK) approximation[6] :

$$\Omega(f) = -\frac{f - f^{eq}}{\lambda} \tag{10}$$

By considering the collision invariant condition (5), it appears that the three moments (2), (3) and (4) still hold if f is replaced by f^{eq}. Then, the non-equilibrium part $(f - f^{eq})$ of the distribution function do not contribute to the macroscopic fluid variables.

2.2 The discrete-velocity Boltzmann equation

Noting that the mass and momentum conservation equations involve moments of up to second order, an effective equilibrium function is obtained[1,21] by a truncation at order 2 of the small velocity Taylor expansion of (9) :

$$f^{eq} = \rho \frac{1}{(2\pi\theta)^{D/2}} \exp\left[-\frac{|\mathbf{c}|^2}{2\theta}\right] \cdot \left\{1 + \frac{\mathbf{c}\cdot\mathbf{u}}{\theta} + \frac{(\mathbf{c}\cdot\mathbf{u})^2}{2\theta^2} - \frac{\mathbf{u}^2}{2\theta}\right\} + O\left(\left(\frac{|\mathbf{u}|}{\sqrt{\theta}}\right)^3\right)$$

Of course, in order to construct a non-isothermal model, a third-order expansion would be considered.[2,8]

As for the original derivation of LBE,[9,29] the polynomial form of the equilibrium function is necessary for the explicit calculation of weighting factors associated with the discrete velocities. As shown in the next section, the evaluation of the stress tensor and heat flux needs the calculation of the third and fourth moments of f^{eq} respectively. Considering the linear form of the equilibrium function, all the integrals (2), (3), (4), (7) and (8) can be expressed as linear combination of terms :

$$\int_{\Re^3} \xi_{x_1}^n \xi_{x_2}^m \xi_{x_3}^p e^{-\left(\xi_{x_1}^2+\xi_{x_2}^2+\xi_{x_3}^2\right)} dx_1 dx_2 dx_3 \ , \quad \boldsymbol{\xi} = \frac{\mathbf{c}}{\sqrt{2\theta}}$$

with $0 \leq n, m, p \leq 7$ in the more general case. The one-dimensional integrals can be calculated using a Gaussian quadrature formulae.[21] If the third-order Hermite formula[12] is used, we obtain :

$$\int_{\Re} \xi_{x_i}^n e^{-\xi_{x_i}^2} dx_i = \sum_{k=1}^{3} \omega_k \xi_k^n \quad \text{for} \quad i = 1, 2, 3$$

where $\xi_{1,2,3} = \left(-\sqrt{3/2}, 0, \sqrt{3/2}\right)$ are the abscissas of the quadrature points with the corresponding weights $\omega_{1,2,3} = (\sqrt{\pi}/6, 2\sqrt{\pi}/3, \sqrt{\pi}/6)$. This quadrature is exact only up to $n = 6$, then it can not be applied for thermal simulations. If we consider now the two-dimensional case ($D = 2$), the moment integrals of the continuous equilibrium function can be evaluated by performing the moment summations over the nine discrete velocities $\mathbf{c}_\alpha = \sqrt{(2\theta)}\,(\xi_k, \xi_l)$ of the discrete-velocity equilibrium functions given by :

$$f_\alpha^{eq} = \frac{\rho h_\alpha}{2\pi\theta}\left\{1 + \frac{\mathbf{c}_\alpha\cdot\mathbf{u}}{\theta} + \frac{(\mathbf{c}_\alpha\cdot\mathbf{u})^2}{2\theta^2} - \frac{\mathbf{u}^2}{2\theta}\right\} \qquad (11)$$

with $h_\alpha = 2\theta\omega_k\omega_l$, $\alpha = 0, ..., 8$. This discretization of the velocity space and the discrete equilibrium function correspond exactly to the classical so-called nine-speed lattice Boltzmann model.[29] Since only the values of distribution functions at the discrete speed are needed for the evaluation of the moments, the continuous Boltzmann equation (1) may be replaced by a discrete-velocity Boltzmann equation :

$$\frac{\partial f_\alpha}{\partial t} + c_{\alpha,i}\frac{\partial f_\alpha}{\partial x_i} = -\frac{1}{\lambda}\left(f_\alpha - f_\alpha^{eq}\right) \qquad (12)$$

Since we are only concerned with isothermal simulations, the energy equation is no more considered in the following. The discrete forms of the density, momentum and stress tensor are :

$$\rho = \sum_{\alpha=0}^{8} f_\alpha \ , \quad \rho\mathbf{u} = \sum_{\alpha=0}^{8} \mathbf{c}_\alpha f_\alpha \qquad (13)$$

and

$$P_{ij} = \sum_{\alpha=0}^{8} \left(c_{\alpha,i} - u_i\right)\left(c_{\alpha,j} - u_j\right) f_\alpha \qquad (14)$$

The continuous moments of f can be evaluated by the discrete moments of $f(\mathbf{x}, \mathbf{c}_\alpha, t) = f_\alpha(\mathbf{x}, t)$ at the velocity nodes because in the limit of slow variations in space and time of the distribution function around the equilibrium state, f can be expressed as a function of f^{eq}. This important result is shown in the next section.

2.3 Derivation of the Navier-Stokes equations

The treatment of the closure problem generally appeals to the expansion of the distribution function as regard to the Knudsen number of the flow. The Knudsen number is the ratio of the collision mean free path to the macroscopic length scale :

$$\epsilon = \frac{\lambda_0\sqrt{\theta_0}}{L}$$

where λ_0 is a characteristic relaxation time (the average time between collisions), θ_0 is the characteristic temperature and L is the hydrodynamic length scale. Considering the dimensionless variables $\hat{t} = t\sqrt{\theta_0}/L$, $\hat{\lambda} = \lambda/\lambda_0$, $\hat{x} = x/L$, $\hat{\mathbf{c}} = \mathbf{c}/\sqrt{\theta_0}$ and $\hat{f}_\alpha = f_\alpha/\rho_0$ the following rescaled Boltzmann equation can be written :

$$\frac{\partial \hat{f}_\alpha}{\partial \hat{t}} + \hat{c}_{\alpha,i}\frac{\partial \hat{f}_\alpha}{\partial \hat{x}_i} = -\frac{1}{\epsilon\hat{\lambda}}\left(\hat{f}_\alpha - \hat{f}_\alpha^{eq}\right) \qquad (15)$$

For simplicity, all hats will be dropped in the following. The Chapman-Enskog or Hilbert expansion allows to find successive approximate solutions of equation (15) in term of small parameter ϵ. The formal expansion of f_α is :

$$f_\alpha = f_\alpha^{(0)} + \epsilon f_\alpha^{(1)} + \epsilon^2 f_\alpha^{(2)} + ... \qquad (16)$$

Inserting (16) in (15) and balancing order by order in ϵ leads to :

$$\text{Order -1 :} \qquad f_\alpha^{(0)} = f_\alpha^{eq} \tag{17}$$

$$\text{Order 0 :} \qquad \frac{\partial f_\alpha^{(0)}}{\partial t} + c_{\alpha,i}\frac{\partial f_\alpha^{(0)}}{\partial x_i} = -\frac{1}{\lambda} f_\alpha^{(1)} \tag{18}$$

$$\text{Order 1 :} \qquad \frac{\partial f_\alpha^{(1)}}{\partial t} + c_{\alpha,i}\frac{\partial f_\alpha^{(1)}}{\partial x_i} = -\frac{1}{\lambda} f_\alpha^{(2)} \tag{19}$$

In the Chapman-Enskog analysis[7] the distribution function is supposed to be a normal solution, which is constrained by :

$$\sum_\alpha \Psi_{\alpha,p} f_\alpha^{(n)} = 0 \qquad n = 1, 2, ... \tag{20}$$

Considering only the first order expansion of f_α, we remark that in case of the BGK collision operator, the solvability condition for $f_\alpha^{(1)}$ is ensured by construction and traduces the conservation of collision invariants (equation (5)). In the general mathematical approach,[4,15,19] the solvability condition (20) for $f_\alpha^{(n)}$ is viewed as a compatibility condition to ensure the existence of the next term $f_\alpha^{(n+1)}$ of the expansion. The interest of equations (17), (18) and (19) is that they provide an explicit expression of the $(n+1)$-th order term of the expansion of f_α as a function of the n-th order term.
Taking the first two moments, $\sum \Psi_{\alpha,p}(\cdot)$ for $p = 0, ..., 2$, of the equation (15) truncated at the order zero and using relation (17) and (20) for $n = 1$, we immediately obtain the mass and momentum conservation equations (6) with :

$$P_{ij}^{(0)} = \sum_\alpha (c_{\alpha,i} - u_i)(c_{\alpha,j} - u_j) f_\alpha^{eq} = \rho\theta\delta_{ij} \tag{21}$$

The details of the calculations of $P_{ij}^{(0)}$ can be found in reference [23]. Noting that the thermodynamic pressure is $p = \rho\theta$ (equation of state of an ideal gas), the exact Euler equations have been recovered by this procedure. Now, if we take the first two moments of the rescaled Boltzmann equation, neglecting term in $O(\epsilon^2)$ and using (20) for $n = 1, 2$ we obtain the conservation equations with :

$$P_{ij} = \sum_\alpha (c_{\alpha,i} - u_i)(c_{\alpha,j} - u_j)\left(f_\alpha^{(0)} + \epsilon f_\alpha^{(1)}\right) \tag{22}$$

Inserting relations (17), (18) and (21), the stress tensor becomes :

$$P_{ij} = p\delta_{ij} - \epsilon\lambda\left(\frac{\partial}{\partial t}\sum_\alpha c_{\alpha,i}c_{\alpha,j}f_\alpha^{eq} + \frac{\partial}{\partial x_k}\sum_\alpha c_{\alpha,i}c_{\alpha,j}c_{\alpha,k}f_\alpha^{eq}\right)$$

The temporal derivative $\partial/\partial t \sum c_{\alpha,i}c_{\alpha,j}f_\alpha^{eq} = \partial/\partial t\,(\rho\theta\delta_{ij} + \rho u_i u_j)$ is calculated as a function of spatial derivatives using the mass and momentum conservation equations at the Euler level. Since the energy conservation equation is not considered, the temperature must be supposed to be constant. The third-order moment can be calculated using the symmetry properties of the discrete velocity system.[23] The final expression of the stress tensor for the isothermal flow is :

$$P_{ij} = p\delta_{ij} - \epsilon\lambda\left(\rho\theta\left(\frac{\partial u_i}{\partial x_j} + \frac{\partial u_j}{\partial x_i}\right) - \frac{\partial \rho u_i u_j u_k}{\partial x_k}\right)$$

The unphysical cubic nonlinear term in the stress tensor can be neglected in case of low Mach flows. More complicated lattice Boltzmann models have been proposed in order to remove this spurious term.[30] The small Mach number hypothesis was also used for the Taylor expansion of the equilibrium function. Then, we can conclude that the Navier-Stokes equation can be derived from the discrete-velocity Boltzmann equation with an accuracy of $O(\epsilon^2)$ and $O(\mathrm{Ma}^3)$. The viscous stress tensor is given by :

$$\tau_{ij} = 2\mu S_{ij} + \left(\eta - \frac{2}{3}\mu\right) S_{kk}\delta_{ij}$$

with $S_{ij} = (\partial u_i/\partial x_j + \partial u_j/\partial x_i)/2$. The shear viscosity is $\mu = \tau\rho\theta$, with $\tau = \epsilon\lambda$. The density-dependent behavior of μ could be removed by noting that in dilute gas, the collision time-scale τ is inversely proportional to the local density.[14] Unlike in usual fluid as air (Stoke's hypothesis), the second viscosity coefficient $\eta = 2\mu/3$ (sometimes called bulk viscosity) is nonzero. This difference directly results from the isothermal hypothesis.[14]

2.4 Integration of the discrete-velocity Boltzmann equation

To achieve a fully discrete lattice Boltzmann equation, we must approximate (15) in $\mathbf{x}$ and t. For example, the discrete-velocity Boltzmann equation can be calculated numerically using an Euler time step in conjunction with a first order upwind spatial discretization.[36] A Lagrangian behavior is then obtained by imposing $\Delta x/\Delta t = |\mathbf{c}_\alpha|$. But this approach does not allow to show that the LBM is in fact a second order method. In the classical approach of the LBM,[9,10,29] the second order accuracy is theoretically shown by Taylor expanding in time and space the kinetic discrete equation (equation (25)). In the framework of Chapman-Enskog procedure, both the temporal derivative operator and the distribution functions are expanded as a function of the Knudsen number.[2,10,23] At the Navier-Stokes level, it appears that the numerical diffusion due to second order

terms can be included in the viscous tensor. The result is that the coefficient τ in the transport coefficients is simply replaced by $\tau - 1/2$. Thus, the numerical contribution to the viscosity for the lattice Boltzmann scheme is negative, requiring that the relaxation time τ to be greater than one half to maintain positive viscosity.

Recently, Dellar[14] showed that the second order accuracy of the LBE and the effective value of the relaxation time could be recovered directly from the discrete-velocity Boltzmann equation. The idea is to integrate equation (15) along the characteristic (the direction of $\mathbf{c}_\alpha$) for a time interval Δt. The integral of the BGK collision operator is approximated by the trapezium rule which is a second order accuracy method :

$$\begin{aligned} & f_\alpha(\mathbf{x}+\mathbf{c}_\alpha\Delta t, t+\Delta t) - f_\alpha(\mathbf{x},t) = \\ & -\frac{\Delta t}{2\tau}\{f_\alpha(\mathbf{x}+\mathbf{c}_\alpha\Delta t, t+\Delta t) - f_\alpha^{eq}(\mathbf{x}+\mathbf{c}_\alpha\Delta t, t+\Delta t) \\ & \qquad + f_\alpha(\mathbf{x},t) - f_\alpha^{eq}(\mathbf{x},t)\} + O\left(\Delta t^3\right) \end{aligned} \tag{23}$$

This equation is implicit because of the presence of the term $f_\alpha^{eq}(\mathbf{x}+\mathbf{c}_\alpha\Delta t, t+\Delta t)$. By a change of variables

$$g_\alpha(\mathbf{x},t) = f_\alpha(\mathbf{x},t) + \frac{\Delta t}{2\tau}\left(f_\alpha(\mathbf{x},t) - f_\alpha^{eq}(\mathbf{x},t)\right) \tag{24}$$

we can find an equivalent explicit equation :

$$g_\alpha(\mathbf{x}+\mathbf{c}_\alpha\Delta t, t+\Delta t) = \left(1-\frac{\Delta t}{\tau_g}\right) g_\alpha(\mathbf{x},t) + \frac{\Delta t}{\tau_g} g_\alpha^{eq}(\mathbf{x},t) \tag{25}$$

with $\tau_g = \tau + \Delta t/2$ and $g_\alpha^{eq} = f_\alpha^{eq}$. For the calculation of the moments of g_α, it is interesting to note that, at the first order in ϵ, we can write $g_\alpha = f_\alpha + \epsilon\Delta t f_\alpha^{(1)}/2\tau$. Then, the first two moments of g_α give exactly to the same macroscopic density and momentum than f_α. Solving the distribution functions g_α by equation (25) with a relaxation time τ_g allows to calculate the fluid variables for a flow of which the distribution functions f_α are described by the discrete-velocity Boltzmann equation (15) with the relaxation time τ. In particular, the kinematic viscosity of the simulated flow is $\nu = \theta(\tau_g - \Delta t/2)$.

2.5 Spatial and temporal discretizations

In this part, we write again the dimensionless variables with hat. The time $\hat{t}$ is discretized with a time step $\hat{\Delta t}$ and a space grid is defined such as if $\hat{\mathbf{x}}_k$ is a grid node then $\hat{\mathbf{x}}_k + \hat{\mathbf{c}}_\alpha\hat{\Delta t}$, $\alpha = 0, ..., 8$ are also on the lattice. In case of the two-dimensional nine speed model (see part 2.2), this condition leads to a mesh with square cells of length $\hat{\Delta x} = \sqrt{3\hat{\theta}}\hat{\Delta t}$. This shows that temperature must be supposed constant. Thermal simulations can not be performed with a "single energy" discrete velocity scheme. To include temperature variations, it is necessary to use a multispeed model.[2,8,10]

We can re-write the relation between time and space increments in term of variables with physical dimension :

$$c_s = \frac{1}{\sqrt{3}}\frac{\Delta x}{\Delta t} \tag{26}$$

where $c_s = \sqrt{\theta}$ is the speed of sound for an "athermal" fluid. The kinematic viscosity also depends on the space and time increments :

$$\nu = \frac{1}{3}\left(\tilde{\tau}_g - \frac{1}{2}\right)\frac{\Delta x^2}{\Delta t} \quad \text{with} \quad \tilde{\tau}_g = \frac{\tau_g}{\Delta t} \tag{27}$$

However, the lattice Boltzmann equation (25) is calculated in its dimensionless form. Using the relation between Δx, Δt and θ, the discrete equilibrium distribution functions given by (11) can be written as :

$$\hat{g}_\alpha^{eq} = \hat{\rho}\tilde{h}_\alpha\left\{1 + 3\tilde{\mathbf{c}}_\alpha\cdot\tilde{\mathbf{u}} + \frac{9}{2}\left(\tilde{\mathbf{c}}_\alpha\cdot\tilde{\mathbf{u}}\right)^2 - \frac{3}{2}\tilde{\mathbf{u}}^2\right\} \tag{28}$$

where $\tilde{\mathbf{u}} = \mathbf{u}\Delta t/\Delta x$ and $\tilde{\mathbf{c}}_\alpha = (0,0)$ for $\alpha = 0$, $\tilde{\mathbf{c}}_\alpha = (\sin((\alpha-1)\pi/2), \cos((\alpha-1)\pi/2))$ for $\alpha = 1,2,3,4$, $\tilde{\mathbf{c}}_\alpha = \sqrt{2}(\sin((2\alpha-1)\pi/4), \cos((2\alpha-1)\pi/4))$ for $\alpha = 2,3,4,5$. The corresponding weights are $\tilde{h}_\alpha = 4/9$ for $\alpha = 0$, $\tilde{h}_\alpha = 1/9$ for $\alpha = 1,2,3,4$ and $\tilde{h}_\alpha = 1/36$ for $\alpha = 5,6,7,8$.

3. Boundary Conditions

For a node on a boundary, some of its neighboring nodes lie outside the flow domain. Therefore, the distribution functions associated with the inward-pointing velocities (velocities which are on the directions pointing into the flow) are not defined. In case of the nine-velocity model, there are three unknown distribution functions on a plane boundary. The more simple way to fix these unknown functions for a no-slip wall condition is to use the bounce-back scheme, that was originally taken from the Lattice Gas Automata method[10] : when a particle distribution streams to a wall node, the particle distribution scatters back to the node it came from. Then, the unknown inward-pointing distributions $\hat{g}_\alpha^{in}$ are defined directly from the outward-pointing distributions : $\hat{g}_\alpha^{in} = \hat{g}_\alpha^{out}$, with $\tilde{\mathbf{c}}_\alpha^{in} = -\tilde{\mathbf{c}}_\alpha^{out}$. Unfortunately, it was found that the bounce-back condition is only first-order accuracy scheme. In order to improve the numerical accuracy, other boundary treatments have been proposed. For example, Noble *et al*[27] suggested using the hydrodynamic variables to calculate the unknown distributions (equation (13)). If the fluid velocity is known ($\mathbf{u} = 0$ for a no-slip wall) it is necessary to enforce a pressure constraint to obtain a system of three equations with three unknowns. The

pressure enforcing can be avoided by adding some supplementary rules on the distribution functions. Zou and He[41] supposed that the bounce-back condition could be apply for the non-equilibrium part of the particle distribution normal to the boundary. If the components of the fluid velocity must also been calculated (frictionless wall, fluid boundary conditions), extrapolation schemes can be used to evaluated some particle distributions[26] or macroscopic fluid variables[41] in order to obtain as many equations as unknowns.

3.1 An extended equilibrium distribution for wall boundary conditions

As it is done for the initialization of populations, the inward-pointing distributions $\hat{g}_\alpha^{in}$ can also be supposed equal to the equilibrium values $\hat{g}_\alpha^{eq}$ which are known in term of $\hat{\rho}$ and $\tilde{\mathbf{u}}$ (equation (28)). In fact, this method for evaluating the unknown distributions can be considered as an application of the lattice Boltzmann equation (25) with $\tilde{\tau}_g = 1$. Therefore, a systematic error is made on the viscous fluxes at the boundary if the relaxation time in the fluid domain is not equal to one. But it can be shown[14,35,39] that the transport coefficients can be controlled independently of the relaxation time by adding "non-equilibrium" terms in the equilibrium populations. For example,[35,39] the following extended equilibrium distribution functions can be used :

$$\hat{g}_\alpha^{eq*} = \hat{g}_\alpha^{eq} + \epsilon\hat{\rho}\left(r\left(\alpha\right)\tilde{c}_{\alpha,i}\tilde{c}_{\alpha,j}\frac{\partial\tilde{u}_i}{\partial\tilde{x}_j} + s\left(\alpha\right)\frac{\partial\tilde{u}_i}{\partial\tilde{x}_i}\right)$$

with $r\left(0\right) = 0$ and $s\left(0\right) = s_0$; $r\left(\alpha\right) = r_1$ and $s\left(\alpha\right) = s_1$ for $\alpha = 1, 2, 3, 4$; $r\left(\alpha\right) = r_2$ and $s\left(\alpha\right) = s_2$ for $\alpha = 5, 6, 7, 8$. Using the symmetric properties of the discrete velocity tensors, it appears that the momentum is conserved by this new expression of the equilibrium distributions while the condition $s_0 + 4s_1 + 4s_2 + 2r_1 + 4r_2 = 0$ is necessary for the mass conservation. Recalling that $\hat{f}_\alpha^{eq*} = \hat{g}_\alpha^{eq*}$, the modified stress tensor can be calculated with equation (22). Neglecting terms in $O\left(\epsilon^2\right)$ and choosing $r_2 = r_1/4$, the viscous stress tensor can be written as :

$$\tilde{\tau}_{ij}^* = 2\hat{\rho}\left(\tilde{\nu} - \epsilon r_2\right)\tilde{S}_{ij} - 2\epsilon\left(r_2 + s_1 + 2s_2\right)\tilde{S}_{kk}\delta_{ij}$$

On a boundary, $\tilde{\tau}_g$ can be set equal to one and the coefficients $\epsilon r\left(\alpha\right)$ and $\epsilon s\left(\alpha\right)$ are calculated such that $\tilde{\nu} - \epsilon r_2$ is equal to the shear viscosity of the inside fluid and $2\epsilon\left(r_2 + s_1 + 2s_2\right) = 0$. The parameter ϵs_2 is freely chosen $\epsilon s_2 = \epsilon s_1/4$ for simplicity. The coefficient ϵs_0 is calculated by the mass conservation condition. This approach for the calculation of inward-pointing distributions requires the macroscopic fluid variables be known on the boundary. In case of a plane boundary parallel to a Cartesian axis, the density does not depend on the inward-pointing distributions (equation (13)) :

$$\hat{\rho} = \frac{1}{1 - \mathbf{n}\cdot\tilde{\mathbf{u}}}\left(\hat{g}_0 + \sum_{\alpha_\parallel}\hat{g}_\alpha + 2\sum_{\alpha^{out}}\hat{g}_\alpha\right)$$

where $\mathbf{n}$ is the inward-pointing normal of the boundary and $\alpha_\parallel$ are the indices of the velocities that are parallel to the boundary. For example, if $\mathbf{n} = (0, 1)$, then $\alpha_\parallel = 1, 3$ and $\alpha^{out} = 4, 7, 8$. In our simulations, the calculation of inward-pointing populations by the extended equilibrium method is only made on no-slip walls. The nonzero velocity gradients are computed using second order asymmetric finite differences. For fluid boundaries where the velocity is not imposed, an other method must be used.

3.2 Finite difference method for non-reflective boundary conditions

In lattice Boltzmann literature, it does not exist boundary scheme to model non-reflective boundary condition for vortical and acoustic perturbations. In this case, six variables must be evaluated : the three inward-pointing distribution functions and the three macroscopic variables. Since the explicit relaxation/convection algorithm (25) can not be applied for inward-pointing populations, the idea is to integrate directly the discrete-velocity Boltzmann equation (15) using classical time and space integration schemes. This approach has been already applied for the calculation of the whole bulk flow using finite difference[31] or finite volume[40] schemes. But since the relation (24) between the distributions $\tilde{g}_\alpha$ and $\tilde{f}_\alpha$ is known, an hybrid method for the boundary treatment can be constructed. An explicit fourth-order Runge-Kutta time-marching is chosen.[38] The spatial derivatives are evaluated with second order central and asymmetric finite differences. Since the distribution functions of the inner points are not calculated with the Runge-Kutta scheme, their values at the intermediate times of the time-step are unknown. Then, the asymmetric finite differences that are used to calculated the normal spatial derivative at the boundary are only introduced in the last step of the temporal integration procedure. For example, we can write the numerical scheme for a boundary parallel to the x-axis :

$$\tilde{f}_\alpha^k = \tilde{f}_\alpha^{k-1} + a_k\left(\Omega^{k-1} - \tilde{c}_{\alpha,x}\frac{\partial\tilde{f}_\alpha^{k-1}}{\partial\tilde{x}}\right) \quad \text{for } k = 1, .., 3$$

$$\tilde{f}_\alpha\left(\tilde{\mathbf{x}}, \tilde{t} + 1\right) = \tilde{f}_\alpha^0 + a_4\left(\Omega^3 - \tilde{c}_{\alpha,x}\frac{\partial\tilde{f}_\alpha^3}{\partial\tilde{x}} - \tilde{c}_{\alpha,y}\frac{\partial\tilde{f}_\alpha^0}{\partial\tilde{y}}\right)$$

with

$$\tilde{f}_\alpha^0 = \tilde{f}_\alpha\left(\tilde{\mathbf{x}}, \tilde{t}\right) \quad \text{and} \quad \Omega^k = -\frac{\tilde{f}_\alpha^k - \tilde{f}_\alpha^{eq,k}}{\tilde{\tau}}$$

The coefficients of the Runge-Kutta method are $a_1 = 1/4$, $a_2 = 1/3$, $a_3 = 1/2$, $a_4 = 1$. Unfortunately, the asymmetric finite difference scheme applied to normal component of the inward-pointing function gradient is a downwind scheme that is unconditionally unstable. It is therefore necessary to suppose that

$$\frac{\partial \tilde{f}_\alpha^{in}}{\partial n} = 0 \tag{29}$$

Moreover, Reider[31] showed that the stability condition for a direct discretization of equation (15) is not imposed by the classical CFL requirement but instead by the constraint that populations are not allowed to evolve far from equilibrium. Then the time-step must be preferably lower than the collision time, or at least we must have $\Delta t = O(\tau)$. Since we are interesting in high Reynolds number and low Mach number flows, this condition is very restrictive and can be overcome by using a space dependent collision time. In the bulk flow, the value of $\tilde{\tau}_g$ is close to $1/2$ in order to reach low viscosity and on fluid boundaries, a minimal value of $\tilde{\tau}_g = 1$ can be imposed. To ensure the continuity, an exponential increase of $\tilde{\tau}_g$ on the nearest boundary nodes is defined.

Even if the condition (29) is not a physical constraint, the boundary treatment described above appears to be a comparatively effective scheme to model non-reflective conditions. For example, the figure 1 shows the behavior of this boundary condition under acoustic excitation (see part 5 for the details of the calculation). The total amplitude of the outcoming wave is about 20 Pa. Only the contour-lines -1 and -2 Pa are altered by the spurious incoming waves. It can be deduced that the reflection rate is about 10%.

4. Short wave damping with artificial viscosity

In this paper, the simulated fluid is air with $\rho_0 = 1.22$ kg/m^3, $c_s = 340$ m/s and $\nu = 1.5 \times 10^{-5}$ m^2/s. Expressions (26) and (27) show that the time and space increments are inversely proportional to $\tilde{\tau} = \tilde{\tau}_g - 1/2$. Consequently, for a given number of lattice node, the Reynolds number of the flow can be increased only by decreasing $\tilde{\tau}_g$ toward $1/2$. But it is well known[36] that the system can become unstable when the lattice relaxation time is close to $1/2$. Most of time, the computation diverges when some high frequency oscillations become too strong. These oscillations can be associated

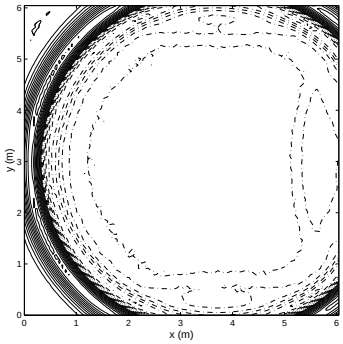

Figure 1: Pressure isocontour of a pulse in uniform flow at $M = 0.2$. $\tilde{\tau} = 1.25 \times 10^{-6}$ and $\tilde{t} = 100$. The domain size is 100×100. ——— positive contours. — · — · negative contours. The pressure step between two contour-lines is 1 Pa.

to unphysical spurious invariants[28] and are generated in under-resolved regions.[14] Then numerical instabilities are generated when there is a lack of spatial resolution in a strongly-sheared region of the flow. In order to perform simulations at high Reynolds number, the numerical oscillations must be damped.[14] In our model, these high frequency instabilities are reduced by applying a selective viscosity filter[37] on the macroscopic variables $\tilde{v} = \hat{\rho}$, $\tilde{u}_x$ and $\tilde{u}_y$:

$$\tilde{v}\left(\tilde{x}, \tilde{y}\right) = \tilde{v}\left(\tilde{x}, \tilde{y}\right) - \tilde{\nu}_a \sum_{j=-3}^{j=3} \left(d_j \tilde{v}\left(\tilde{x}+j, \tilde{y}\right) + d_j \tilde{v}\left(\tilde{x}, \tilde{y}+j\right)\right)$$

where $\tilde{\nu}_a$ is the artificial viscosity. Another solution proposed by Dellar[14] is to use an enhanced bulk viscosity. Indeed, the bulk viscosity can be readily adjusted by using the extended equilibrium functions (see part 3.1).

5. Pulse propagation in a uniform flow

Simulations of sound waves with LBM were studied previously[5,14] but with an emphasis on non-linear steepening at finite amplitude[5] and energy decay of high frequency plane waves due to viscous dissipation.[5,14] For very small values of $\tilde{\tau}$, it is possible to simulate low frequency wave with a limited number of nodes. The viscous dissipation of long wave acoustic perturbations is negligible and the results of LBM computations can be compared to the solutions of Euler equations. For example, the analytical expression of the linear propagation of a Gaussian pressure pulse in a uniform flow is known.[20] A Gaussian density source of half-width b and amplitude $10^{-3}\rho_0$ is introduced at the center of the computational domain. For an Euler problem, numerical oscillations are very weak because the distribution functions are always close to the equilibrium, therefore the artificial viscosity is not applied. Figure 2 shows the

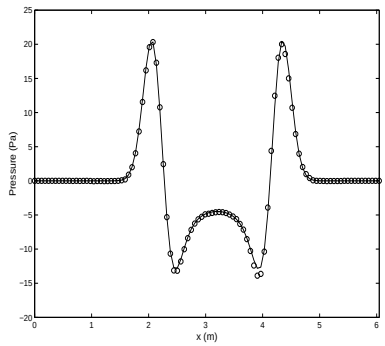

Figure 2: Pressure pulse in a uniform flow at $M = 0.2$. $\tilde{\tau} = 1.25 \times 10^{-6}$ and $\tilde{t} = 30$. The domain size is 100×100. ——— Analytical solution. ∘ LBM simulation.

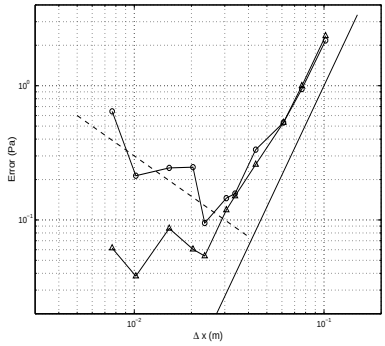

Figure 3: Evolution of the error as a function of Δx. ∘ Error at a given physical time. △ Error at a given lattice time ($\tilde{t} = 20$). ——— line with slope = 3. – – – line with slope = −1.

pressure profile along the centerline of the domain for a convection flow at $M = 0.2$. The agreement between the analytical and calculated profiles is quite good. Using the reference analytical solution p_{ref}, the convergence of the numerical method can be investigated as a function of the lattice discretization. Since the time and spatial steps are linearly linked by (26), the accuracy is only expressed in term of Δx. The constant CFL number is a characteristic of LBM and must be taken account for the convergence study.[31] Indeed, a smaller spatial lattice size requires an increase in the number of time iteration needed for the same flow evolution.

The half-width of the pulse and the domain size are kept constant at $b = 19.3$ cm and $N_x \times N_y = 16\,(b \times b)$. The definition of the error norm is :

$$Err = \left(\frac{1}{N_x} \sum_{k=1}^{N_x} \left(p\left(k, N_y/2\right) - p_{ref} \right)^2 \right)^{1/2}$$

In figure 3, if we consider first the convergence rate for the largest spatial size, we see that the error decay is almost in power three. This result is in agreement with equation (23). However, the error saturates at a certain level as the mesh is refined and even increases if the error is measured at a given physical time. The linear error increase is due to the cumulative sum of the errors made at each iteration. The convergence saturation of LBM has been also pointed out in previous works.[25,31,35] It can be associated with several effects such as the influence of higher order terms in $O\left(M^3\right)$ and $O\left(\epsilon^2\right)$ (so-called compressibility errors) or the numerical round-off error.[35] Further investigations would be necessary to study the cause of the error saturation in our particular case.

Despite this limitation, the lattice Boltzmann method appears to be a fairly good numerical scheme for acoustic propagation.

6. Simulations of flow-excited cavities

In order to assess the ability of the lattice Boltzmann method to simulate practical flow problems for low subsonic speed and high Reynolds number, we studied the case of a flow-excited cavity. Even if the introduction of a subgrid viscosity for turbulence modeling is not difficult,[22] the two-dimensional hypothesis does not allow to compute actual turbulent phenomenon. Then, laminar flows are chosen in this validation.

6.1 Cavity flow oscillation at very low Mach number

We try to reproduce the experiments of Sarohia[34] who investigated a laminar flow oscillation over an axisymmetric non-resonant cavity. Flow oscillations over rectangular cavities at very low Mach numbers and comparable Reynolds numbers have been also studied by Gharib & Roshko[17] and Rockwell & Knisely.[33] The simulations are performed at $Re_{\theta_0} = 240$ where θ_0 is the momentum thickness of the boundary layer at separation. The Mach number is $M = 0.044$. The depth of the cavity $D/\theta_0 = 80$ is kept constant. A cavity with length to depth ratio $L/D = 1$ is meshed with 50×50 points. The mesh size is 300×200 outside the cavity. The relaxation time is $\tilde{\tau} = 1.6 \times 10^{-4}$ and the artificial viscosity is $\tilde{\nu}_a = 0.1$. The initial condition is a polynomial expression of the laminar Blasius boundary layer. A typical computation is 6 hours long on a SGI workstation with a 250 MHz R10000 processor.

Figure 4 shows the transverse velocity signals obtained with four L/θ_0 ratios. The Strouhal numbers for the simulations at $L/\theta_0 = 61$, $L/\theta_0 = 80$ and $L/\theta_0 = 104$ are respectively $St = fL/U_0 = 0.57$, 0.91 and 1.01. Figure 5 depicts the variation of the phase difference Φ for probes located along the cavity opening near the outside edge of the shear layer. Between the two corners of the cavity, the characteristic phase difference[17] of $2n\pi$ with $n = 1, 2$ is found. Then for $L/\theta_0 = 61$ the flow os-

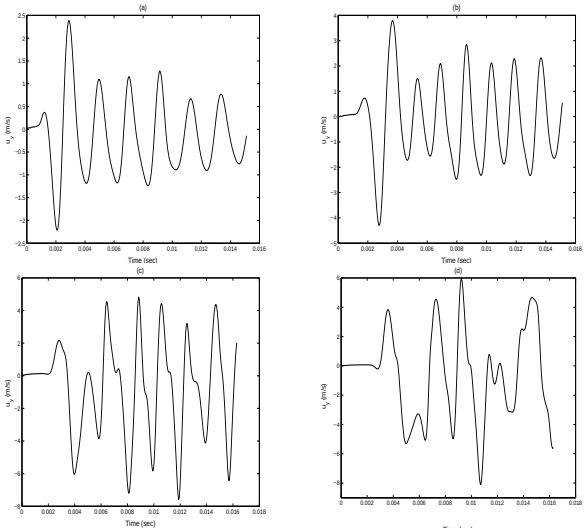

Figure 4: Time history of the transverse velocity for a point at $y/\theta_0 = 1.5$ and (a) $L/\theta_0 = 61$, $x/\theta_0 = 48$; (b) $L/\theta_0 = 80$, $x/\theta_0 = 64$; (c) $L/\theta_0 = 104$, $x/\theta_0 = 93$; (d) $L/\theta_0 = 134$, $x/\theta_0 = 112$.

cillates in mode I and for $L/\theta_0 = 80$ and $L/\theta_0 = 104$ the oscillation is in mode II (figure 6 (a)). This behavior well corresponds to experimental observations.[17,34] For $L/\theta_0 = 61$, the oscillation phenomenon tends to disappear (figure 4). It is consistent with experimental data, where the first mode appears to not be a stable stage of oscillation in certain conditions. As L/θ_0 further increases, the transition from mode II to mode III is obtained for $L/\theta_0 = 122$ in experiments.[17] Then for $L/\theta_0 = 134$, the flow normally oscillates in mode III while temporal signal (figure 4) and flow visualization (figure 6 (b)) indicates that the cavity flow is in the wake mode.[17] This non-coherent organization of the flow only appears at $L/\theta_0 = 160$ in experiments. The transition to wake mode for too low ratios L/θ_0 has been also observed in other numerical simulations[11] for Mach numbers between 0.4 and 0.8 and is probably due to the two-dimensional hypothesis of the computations.

For the self-sustained oscillation conditions, the growth of the momentum thickness θ of the shear layer have been measured. As in experimental studies,[17,33,34] θ is found to grow linearly with x/θ_0 and for all cases, the growth rate is almost constant at $d\theta/dx = 0.021$ which is very close to the value found by Sarohia ($d\theta/dx = 0.022$). Figure 7 represents the streamwise evolution of the transverse profile of the shear stress for $L/\theta_0 = 80$. The amplitude and the existence of the second peak in the lower portion of the shear layer compare very well with the measurements of Gharib & Roshko.

6.2 The acoustic field radiated by a cavity flow

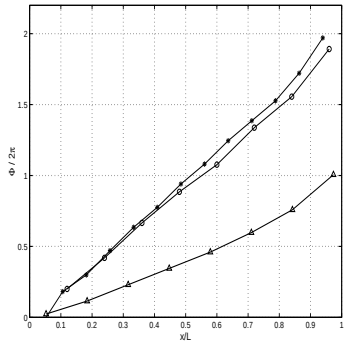

Figure 5: Streamwise variation of the transverse velocity phase at $y/\theta_0 = 6.5$. $\triangle$, $L/\theta_0 = 61$, mode I; $\circ$, $L/\theta_0 = 80$, mode II; $*$, $L/\theta_0 = 104$, mode III.

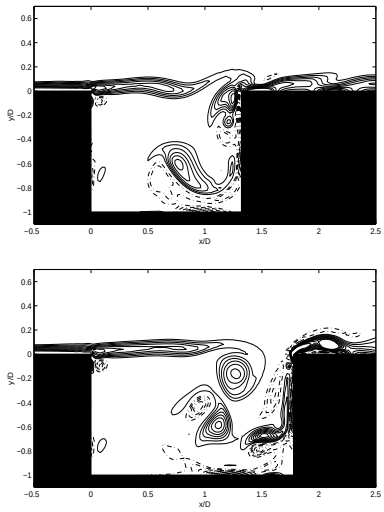

(a)

(b)

Figure 6: Instantaneous vorticity contours. (a) $L/\theta_0 = 104$, mode II; (b) $L/\theta_0 = 134$, wake mode. ——— negative contours; — · — · positive contours.

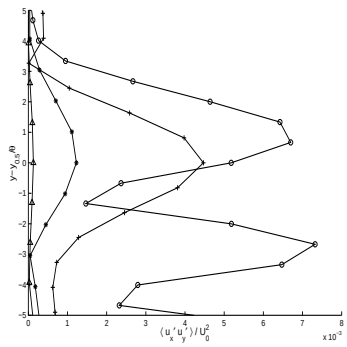

Figure 7: Reynolds stress profiles for $L/\theta_0 = 80$. $\triangle$, $x/\theta_0 = 14$; $*$, $x/\theta_0 = 38$; $+$ $x/\theta_0 = 54$; $\circ$, $x/\theta_0 = 70$.

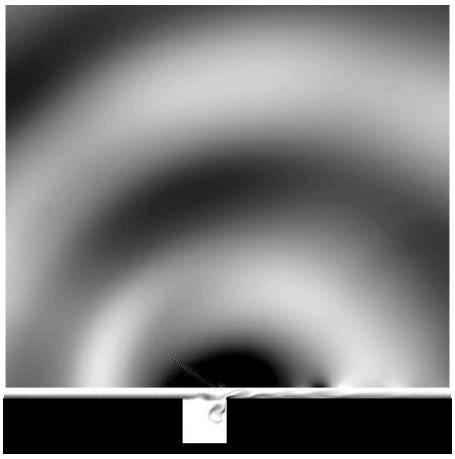

Figure 8: Example of the pressure and vorticity fields produced by an unsteady cavity flow. $L/D = 1$, $L/\theta_0 = 60$, $M = 0.25$. The pressure is drawn for values between -200 and 200 Pa. The negative pressures are in dark gray.

The sound field radiated by a flow-excited cavity can be also calculated by the code. In order to reduced the ratio between the acoustic wavelength and the domain size, calculations are performed with Mach number $M = 0.25$. We keep the parameters $\tilde{\tau}$, $\tilde{\nu}_a$ of the previous computations and a cavity with the same characteristic size is simulated. The outside domain size is inceased up to 500×500 mesh points. the Reynolds number is $Re_{\theta_0} = 2250$. Figure 8 shows the acoustic pressure field radiated by a cavity flow for $L/D = 1$ and $L/\theta_0 = 60$. The oscillation frequency is $fL/U_0 = 0.81$.

For this cavity length-to-depth ratio and Mach number, there is no available numerical data to compare precisely our acoustic field. Most of cavity noise computations have been performed[11,18] for shallow cavities ($L/D \geq 2$) at greater Mach numbers. But, as in these simulations, the acoustic field is centered at the downstream edge of the cavity : the noise is generated by the periodic impingement of coherent vortices upon the corner. Even if the radiated sound of our computation is not omni-directional, the very strong upstream directivity[11,18] is not recovered. This difference can be explained by a lower effect of the free stream convection and a different acoustic inteference pattern inside the cavity.

7. Concluding remarks

In this paper, the lattice Boltzmann method is investigated for aeroacoustic simulations. The recent approach that allows to derive a discrete-velocity Boltzmann equation is presented. The Navier-Stokes equations can be recovered using exactly the same mathematical procedure that is applied in the continuous Boltzmann kinetic theory. The second order accuracy equations of the LBM are found by integrating the discrete velocity model and introducing equivalent population functions: the populations that are calculated by the LBM are not the populations of the discrete velocity equation but give the same macroscopic variables. This procedure allows very large time-steps as regard to the fluid collision time, which is not physically correct if the discrete-velocity Boltzmann equation is directly solved. Specific treatments for aeroacoustic computations at high Reynolds number have been added to the two-dimensional model. With small computational efforts, we obtain a quite good agreement between numerical results and analytical or experimental data. Of course, further validations and comparisons with the other CAA methods would be necessary but this first application of Boltzmann methods for computational aeroacoustics is encouraging. The new explicit link of the LBM to the continuous kinetic theory offers new opportunities for future developments of kinetic boundary conditions[3] and maybe for turbulence modeling.[13]

References

[1] Abe, T., 1997. Derivation of the lattice Boltzmann method by means of the discrete ordinate method for the Boltzmann equation. *J. Comput. Phys.*, **131**, 241-246.

[2] Alexander, F.J., Chen, S. & Sterling, J.D., 1993. Lattice Boltzmann thermohydrodynamics. *Phys. Rev. E*, **47**, R2249.

[3] Ansumali, S. & Karlin, I.V., 2002. Kinetic boundary conditions in the lattice Boltzmann method. *Preprint.*

[4] Bardos, C., Golse, F. & Levermore, D., 1991. Fluid dynamic limits of kinetic equations I : Formal derivations. *J. Stat. Phys.*, **63**, 323-344.

[5] Buick, J.M., Greated, C.A. & Campbell, D.M., 1998. Lattice BGK simulation of sound waves. *Europhys. Lett.*, **43**(3), 235-240.

[6] Cercignani, C., 1988. The Boltzmann equation and its applications. *Spinger Verlag, New York.*

[7] Chapman, S. & Cowling, T.G., 1970. The mathematical theory of non-uniform gases. *Cambridge University Press.*

[8] Chen, H., Teixeira, C. & Molvig, K., 1997. Digital Physics approach to computational fluid dynamics : some basic theoretical features. *Int. J. Mod. Phys. C*, **8**(4), 675-684.

[9] Chen, S., Chen, H., Martinez D. & Matthaeus, W., 1991. Lattice Boltzmann model for simulation of magnetohydrodynamics. *Phys. Rev. Lett.*, **67**, 3776-3779.

[10] Chen, S. & Doolen, G.D., 1998. Lattice Boltzmann Method for fluid flows. *Annu. Rev. Fluid Mech.*, **30**, 329-364.

[11] Colonius, T., Basu, A.J. & Rowley, C.W., 1999. Numerical investigation of the flow past a cavity. *AIAA Paper* **99-1912**.

[12] Davis, P.J. & Rabinowitz, P., 1984. Methods for Numerical Integration. *Academic, New York, 2nd ed.*

[13] Degond, P. & Lemou, M., 2002. Turbulence models for incompressible fluids derived from kinetic theory. *to appear in* J. Math. Fluid Mech.

[14] Dellar, P.J., 2001. Bulk and shear viscosities in lattice Boltzmann equations. *Phys. Rev. E*, **64**, 031203.

[15] Esposito, R., Lebowitz, J.L. & Marra, R., 1999. On the derivation of hydrodynamics from the Boltzmann equation. *Phys. Fluids*, **11**(8), 2354-2366.

[16] Frisch, U., Hasslacher, B. & Pomeau, Y., 1986. Lattice-Gas Automata for the Navier-Stokes equation. *Phys. Rev. Lett.*, **56**(14), 1505-1508.

[17] Gharib, M. & Roshko, A., 1987. The effect of flow oscillations on cavity drag. *J. Fluid Mech.*, **117**, 501-530.

[18] Gloerfelt, X., Bailly, C. & Juvé, D., 2001. Computation of the noise radiated by a subsonic cavity using direct simulation and acoustic analogy. *AIAA Paper* **01-2226**.

[19] Golse, F., 1998. From kinetic to macroscopic models. *Session "L'Etat de la Recherche" de la S.M.F., Orléans*, www.dma.ens.fr/~golse/qcours.html.

[20] Hardin, J.C., Ristorcelli, J.R. & Tam, C.K.W., 1995. Workshop on benchmark problems in computational aeroacoustics. ICASE/LaRC. NASA CP - 3300.

[21] He, X. & Luo, L.-S., 1997. Theory of the lattice Boltzmann method: From the Boltzmann equation to the lattice Boltzmann equation. *Phys. Rev. E*, **56**, 6811-6817.

[22] Hou, S., Sterling, J., Chen, S. & Doolen, G.D., 1996. A lattice Boltzmann subgrid model for high Reynolds number flows. *Fields Inst. Comm.*, **6**, 151-166.

[23] Hou, S., Zou, Q., Chen, S., Doolen, G.D. & Cogley, A.C., 1995. Simulation of cavity flow by the lattice Boltzmann method. *J. Comp. Phys.*, **118**, 329-347.

[24] Huang, K. 1963. Statistical Mechanics. *Wiley, New York.*

[25] Maier, R.S & Bernard, R.S., 1997. Accuracy of the lattice-Boltzmann method. *Int. J. Modern Phys. C*, **8**(4), 747-752.

[26] Maier, R.S, Bernard, R.S. & Grunau, D.W., 1996. Boundary conditions for the lattice Boltzmann method. *Phys. Fluids*, **8**(7), 1788-1801.

[27] Noble, D.R., Chen, S., Georgiadis, J.G. & Buckius, R.O., 1995. A consistent hydrodynamic boundary condition for the lattice Boltzmann method. *Phys. Fluids*, **7**(1), 203-209.

[28] Qian, Y.-H., 1997. Fractional propagation and the elimination of staggered invariants in lattice-BGK models. *Int. J. Modern Phys. C*, **8**(4), 753-761.

[29] Qian, Y.-H., D'Humières, D. & Lallemand, P., 1992. Lattice BGK models for Navier-Stokes equation. *Europhys. Lett.*, **17**(6), 479-484.

[30] Qian, Y.-H. & Zhou, Y., 1998. Complete Galilean-invariant lattice BGK models for the Navier-Stokes equation. NASA/CR-1998-208701, ICASE Report No. 98-38.

[31] Reider, M.B. & Sterling, J.D., 1995. Accuracy of discrete-velocity BGK models for the simulation of incompressible Navier-Stokes equations. *Comput. Fluids*, **24**, 459-467.

[32] Ricot, D., Maillard, V. & Bailly, C., 2001. Numerical simulation of the unsteady flow past a cavity and application to the sunroof buffeting. *AIAA Paper* **01-2112**.

[33] Rockwell, D. & Knisely, C., 1979. The organized nature of flow impingement upon a corner. *J. Fluid Mech.*, **93**(3), 413-432.

[34] Sarohia, V., 1977. Experimental investigation of oscillations in flows over shallow cavities. *AIAA J.*, **15**(7), 984-991.

[35] Skordos, P.A., 1993. Initial and boundary conditions for the Lattice Boltzmann Method. *Phys. Rev. E*, **48**, 4823-4842.

[36] Sterling, J.D & Chen, S., 1996. Stability analysis of lattice Boltzmann methods. *J. Comp. Phys.*, **123**, 196-206.

[37] Tam, C.K.W., Webb, J.C & Dong, Z., 1993. A study of the short wave components in computational acoustics. *J. Comput. Acoust.*, **1**(1), 1-30.

[38] Williamson, J.H., 1980. Low-storage Runge-Kutta schemes. *J. Comput. Phys.*, **35**, 48-56.

[39] Wolfram, S., 1986. Cellular automata fluids 1: Basic theory. *J. Stat. Phys.*, **45**(3), 471-526.

[40] Xi, H., Peng, G. & Chou, S.-H., 1999. Finite-volume lattice Boltzmann schemes in two and three dimensions. *Phys. Rev. E*, **60**(3), 3380-3388.

[41] Zou, Q. & He, X., 1997. On pressure and velocity boundary conditions for the lattice Boltzmann BGK model. *Phys. Fluids*, **9**, 1591-1598.